**Science and Technology Indonesia**
*e*-ISSN:2580-4391 *p*-ISSN:2580-4405
Vol. 10, No. 2, April 2025

Research Paper

# Optimization of Radiation and Electric Current Storage in a Dye-Sensitized Solar-Cell System Based FTO/$TiO_2$/Acy/PVDF/C/FTO Modules for Electrical Equipment Applications

Muhammad Ridho Hafid Kurniawan[1], Sinta Anjas Cahyani[1], Nita Kusumawati[1*], Pirim Setiarso[1], Supari Muslim[2]

[1]*Department of Chemistry, Faculty of Mathematics and Natural Sciences, Universitas Negeri Surabaya, Surabaya, 60231, Indonesia*
[2]*Department of Electrical Engineering, Faculty of Engineering, Universitas Negeri Surabaya, Surabaya, 60231, Indonesia*
***Corresponding author**: nitakusumawati@unesa.ac.id

**Abstract**
Indonesia has an electrification rate exceeding 99% as of 2020, yet it faces increasing electricity demands amid declining fossil fuel availability. Solar energy, particularly through DSSC, presents a promising renewable alternative, benefiting from an abundant radiation potential of up to 120.000 TW. DSSC have garnered significant attention due to their thin design, high efficiency, ease of fabrication, and environmental friendliness. The DSSC module was designed using two FTO glass plates as electrodes, with an anode surface area of 3 $cm^2$. The $TiO_2$ photoanode was prepared using a casting knife technique and then sintered at 450°C for one hour. This was followed by sensitization with anthocyanin dye derived from the butterfly pea flower under acidic conditions for 24 hours to ensure the stability of the compound. The electrolyte system consisted of PVDF NF membranes soaked in the electrolyte solution for one hour to prevent leakage, thus completing the FTO/$TiO_2$/PVDF/C/FTO system. Performance optimization involved arranging 20 DSSC cells in a mixed series-parallel circuit configuration. Electrical parameters were measured using a multimeter under various lamp irradiation durations. The optimal efficiency was achieved with 5 hours of irradiation, resulting in 2.050 mV and $23.5 \times 10^{-3}$ $\mu$A. When integrated into a battery system, the DSSC module demonstrated effective current storage stability over 6 hours, indicating strong potential for practical implementation in sustainable energy generation for real-world applications.

**Keywords**
Butterfly Pea Flower, Current Storage, DSSC, Irradiation, PVDF NF

Received: 18 November 2024, Accepted: 18 February 2025
https://doi.org/10.26554/sti.2025.10.2.574-587

## 1. INTRODUCTION

Along with world population growth, technological developments, and industry, the energy demand worldwide continues to increase by 4.6% per year (Santamouris and Vasilakopoulou, 2021). Generally, energy is obtained through fossil fuels (solid, liquid, or gas) such as natural gas, oil, and coal which further increases the need for fossil energy so that petroleum reserves are getting depleted, it is expected to last only until 2070 (Holechek et al., 2022; Hosseinnezhad et al., 2020). As a non-renewable resource, it takes millions of years to form fossil fuel reserves, and fossil fuels have contributed to an increase in global $CO_2$ emissions by 37.5 billion tonnes by 2023 (Jensen, 2023), accelerating the impact of global warming (Holechek et al., 2022; Hosseinnezhad et al., 2020).

In 2020, Indonesia has an electrification rate exceeding 99% and faces the challenge of increasing energy demand projected to reach 400 TWh by 2025, leading various environmental promotions to begin to be discussed, making world researchers focus research on alternative renewable energy (Kula et al., 2019; Santamouris and Vasilakopoulou, 2021). To minimize the impact of non-renewable resources, solar energy, as the largest source of energy on Earth, can be the most potentially valuable resource (Cakar, 2019; Farghali et al., 2023). It has the criteria of being non-polluting (environmentally friendly), being free in almost all regions of the Earth, having a smart energy grid with high potential interest, having very low operating and maintenance costs (0.3-0.4 USD/kWh), and being easy to install or operate. With an average solar radiation of 4.8 kWh/$m^2$/day and 6-8 hours of irradiation duration, this energy is almost eternal (Jalomo-Cuevas et al., 2023; Kumar et al., 2023; Miettunen and Santasalo-Aarnio, 2021).

Dye-sensitized solar cells (DSSCs) represent a third-generation photovoltaic technology that converts solar energy to electricity through photosensitization, achieving up to 14% efficiency at 25-30% of silicon solar cell manufacturing costs

(Amir-Al Zumahi et al., 2021; Andualem and Demiss, 2018; Dhorkule et al., 2024). The fabrication of DSSC has recently gained significant attention due to its simplicity and cost-effectiveness compared to traditional silicon solar cells with annual efficiency gains of 0.5% attributed to the ongoing optimization of materials and fabrication processes (Bandara et al., 2018; Dhorkule et al., 2024). The DSSC system comprises six essential components: semiconductor photoanode, conductive substrate, counter electrode (cathode), organic dye, electrolyte solution, and sealant (Cakar, 2019; Ozaydin and Gozel, 2023). $TiO_2$ proved to be compatible with fulfilling the demand for sensitive semiconductors as a photoanode due to its optimal band gap, stability, practicality, and cost-effectiveness. Within the DSSC system, the photogalvanic process, the dye absorbs light, leading to photo-excitation and the injection of electrons into the conduction band of the $TiO_2$ semiconductor. The oxidized form of the photosensitizer dye is then regenerated through a redox reaction at the electron interface. This process allows the electrons to travel through an external circuit to reach the counter electrode. LUMO energy level of many dyes located slightly above the conduction band edge of $TiO_2$ which can facilitate electron injection that also facilitates the collection and conduction of electron charge (Bandara et al., 2018; Kumar et al., 2023; Ozaydin and Gozel, 2023).

Transparent conductive oxide (TCO) substrates serve as current collectors and protective covers in DSSC architecture (Miettunen and Santasalo-Aarnio, 2021; Sinha et al., 2018). While indium tin oxide (ITO) is commonly used, its conductivity deteriorates above 200°C (Chen, 2022; Ibrahim et al., 2021). Instead, fluorine-doped tin oxide (FTO) offers superior thermal stability with a lower risk of thermal decomposition on the conductive layer and serves dual functions: on one side, it supports $TiO_2$ paste film applied via the casting knife method and high-temperature treatment to remove the organic binder to achieve pure $TiO_2$ film for enhanced inter-particle binding (Agrawal et al., 2021; Kusumawati et al., 2023; Weldemicheal et al., 2023). The opposite side features catalysts coated on FTO glass by the carbonization method to ensure the catalytic activity of electrons towards electrolyte reduction and electron charge transfer kinetics at the cathode (Ali et al., 2021; Chen, 2022). Carbon-coated FTO glass is an economical alternative to platinum for catalyzing electrolyte reduction at the counter electrode (Ali et al., 2021; Dhanasekaran and Marimuthu, 2022; Kusumawati et al., 2023; Narudin et al., 2021; Tomar et al., 2021).

The photosensitizer must possess characteristics that align with the available light spectrum to function effectively as a solar cell. Different photosensitizers absorb light at varying levels, affecting their efficiency and cost. In this case, the dye photosensitizer plays its main role as a light harvester and electron supplier (Kumar et al., 2023; Kula et al., 2019; Ozaydin and Gozel, 2023). Synthetic inorganic complex compounds, particularly ruthenium/zinc complexes, offer high chemical stability and conversion efficiency (11-12%), but they often contain expensive metals that may pose environmental concerns and limit practical applications (Al-Alwani et al., 2017; Fetouh et al., 2024; Mauri et al., 2021). In contrast, natural organic dyes have emerged as a cost-effective alternative to traditional photosensitizers, serving as effective light absorption media (Erande et al., 2021). Natural dyes, specifically anthocyanin from butterfly pea flower (*Clitoria ternatea* L.), present a sustainable alternative with broad light absorption (350-700 nm), cost-effective extraction, and eco-friendly characteristics (Chandrajith et al., 2021). The anthocyanin pigments facilitate electron injection between LUMO-$TiO_2$ and HOMO-electrolyte systems, making it an important component in DSSC efficiency with promising molar absorptivity of $4.2 \times 10^4$ L $mol^{-1}$ $cm^{-1}$ for DSSC applications (Sathyajothi et al., 2017).

DSSC performance can be influenced by the factors of the electrolyte. In the DSSC, the electrolyte is crucial for enabling charge transport between the photoanode and the counter electrode. Many highly efficient DSSCs have been commonly fabricated using liquid electrolytes containing redox pairs such as $I^-/I_3$ ($I_5$), which are dissolved in a volatile organic solvent. There are significant sealing problems that may limit their practical application, namely hazardous solvent evaporation and liquid electrolyte leaks. Quasi-solid or polymer-based solid-state electrolytes are an extension of the problems that can be caused by liquid electrolytes. Polymer electrolytes provide several advantages, including strong ionic conductivity, superior safety, high tensile strength, simplicity of manufacture, great flexibility, and no leakage (Sundaramoorthy et al., 2018).

Poly(vinylidene fluoride) (PVDF) is a polymer employed as a porous separator or gel polymer electrolyte matrix in this study, due to its excellent electrochemical stability and high mechanical strength compared to other polymers, as well as the evenly distributed pore structure on this PVDF membrane, which supports the trapping of electrolyte solution so that electron transfer in the DSSC system can work optimally (Kumar et al., 2023; Kusumawati et al., 2024; Kusumawati et al., 2018b; Kusumawati et al., 2018a). However, PVDF membranes have hydrophobic properties that can reduce the ionic mobility of $I^-/I^{3-}$ ions in PVDF. To increase the mobility of the electrolyte polymer, this research uses electrospinning to fabricate a PVDF nanofiber (PVDF-NF) membrane as a solution to this problem. The amfort structure dominates the PVDF-NF membrane, which can provide better ionic conductivity than the PVDF membrane (Kusumawati et al., 2024).

DSSC efficiency is shown in the measurement of current and voltage using a multimeter, with lamp irradiation in several variations of irradiation time. Since 1980, efficiency charts of different types of solar cells were released by the National Renewable Energy Laboratory (NREL, USA), showing a yearly graph of DSSC development focused on improving device performance by reducing manufacturing costs (Source: `https://www.nrel.gov/pv/cell-efficiency.html`). Standard irradiation with lamps is required for planned use indoors. This study presents a comprehensive examination of how the light source spectrum utilized for DSSC illumination influences the energy conversion efficiency of the cell. When light in the form

of photons hits the DSSC cell, the energy from the photons is absorbed by the dye photosensitizer extract (Vidana Gamage et al., 2021). The variation of lamp irradiation time is carried out to test the current and voltage resistance of the PVDF polymer electrolyte DSSC to produce optimal current and voltage because there is no electrolyte evaporation factor when the DSSC temperature increases.

The current and voltage generated by DSSC modules are typically low, but higher levels are needed for efficient energy applications. One solution is to store the generated current and voltage in a battery, which maintains storage stability. By varying the storage duration, longer times lead to greater current and voltage retention. This is influenced by lighting, as increased lamp irradiation enhances photosensitizer performance, resulting in higher electrical parameters for the DSSC module (Twitchell et al., 2023).

In this study, DSSC module performance is optimized through the comprehensive development of a PVDF-NF membrane electrolyte integrated with butterfly pea flower (*Clitoria ternatea* L.) extract as a natural photosensitizer. The research focuses on the design of a novel multi-cell DSSC module with both series and parallel configurations, investigating the effects of irradiation duration on electrical output parameters and evaluating energy storage system efficiency for practical device applications. The DSSC architecture employs a sandwich structure comprising FTO glass layers, $TiO_2$-anthocyanin photosensitizer, and carbon counter electrode, with the PVDF NF polymer electrolyte membrane serving as a crucial stabilizing component. Comprehensive characterization includes analysis of PVDF NF functional groups, anthocyanin UV absorption at pH 1, and PVDF NF membrane morphology through SEM. The scientific merit lies in addressing key limitations of conventional electrolyte systems through PVDF NF membrane implementation, targeting enhanced cell stability and durability with conversion efficiencies of 5-7%. This integrated approach, combining optimized polymer membrane technology with natural dye extraction in a scalable module system, presents a promising pathway toward practical DSSC implementation through systematic optimization of irradiation parameters, circuit configuration, and storage efficiency.

## 2. EXPERIMENTAL SECTION

### 2.1 Materials

The material specifications in this study include $TiO_2$ (21 nm nanopowder; 99.5%) from Sigma Aldrich, China; acetone (≥99.5%), $HNO_3$ (63%), and polyethylene glycol (PEG) (Mw 1000) from Sigma Aldrich, Germany; KI (≥99%), N, N-Dimethylacetamide (DMAc) (≥99%) from Merck, Belgium; propylene carbonate (PC) (99.7%; anhydrous), ethylene carbonate (EC) (99%; anhydrous) from Sigma Aldrich, USA; Tween-80 from PT. Brataco Chemika, Indonesia; Iodine-(≥99.8%), PVDF powder (Mw ~534,000) from Sigma Aldrich, Singapore; and FTO glass (resistivity 10) from Changchun Yutai Optics Co., Ltd, China

### 2.2 Methods

#### 2.2.1 Pasta $TiO_2$

A mixture was created by combining 0.2 grams of $TiO_2$, 0.08 grams of PEG-1000, 0.4 mL of a 0.1 M $HNO_3$ solution, and 0.05 mL of Tween-80. This mixture was then stirred at a speed of 100 rpm for 30 minutes, resulting in the preparation of pasta $TiO_2$.

#### 2.2.2 Natural Photosensitizer

The maceration method was employed to create a natural dye sensitizer. The specific natural dye sensitizer utilized in this process was derived from dried butterfly pea flowers. To begin, the dried butterfly pea flowers were soaked in distilled water at a ratio of 1:6. The filtrate obtained from maceration was then subjected to evaporation with a Buchi R-300 rotary evaporator. The concentrated solution obtained from evaporation was subsequently stored in a freezer at a temperature of -4°C.

#### 2.2.3 Polymer-Electrolyte Membrane

To create a polymer-electrolyte membrane, the process involves 2 steps: preparing an electrolyte solution and producing a PVDF NF membrane. The electrolyte solution consists of 9.2 mg $I_2$, 0.06 g KI, 0.4 g EC, and 0.4 g PC, mixed with a magnetic stirrer at 100 rpm for 30 minutes. For the PVDF membranes, electrospinning is used, with PVDF dissolved in a 3:2 mixture of DMAc and acetone, heated to 65°C and stirred at 270 rpm for 12 hours, resulting in an 18% (w/v) PVDF solution. After that, PVDF NF was created by ejecting an 18% PVDF solution with electrospinning Nacriebe 200 at a distance of 15 cm, a voltage of 15 kV, and a flow rate of 1 mL per hour.

#### 2.2.4 Characterization

The absorption spectra of anthocyanin were analyzed using UV-Vis spectrophotometry (Shimadzu UV-1800) in the wavelength range of 200-800 nm. Fourier Transform Infrared (FTIR) of PVDF NF membrane used in DSSC is analyzed using Perkin Elmer (FTIR) Spectrum Two. The surface morphology of the PVDF NF membrane was examined using Scanning Electron Microscopy (SEM, FEI Inspect S50).

#### 2.2.5 Module DSSC

The DSSC is composed of two FTO glass plates with a surface area of 3 $cm^2$, one serving as the anode and the other as the cathode. To prepare the $TiO_2$ photoanode, a layer of $TiO_2$ paste was applied to the glass using a casting knife technique. The coated glass was then heated at 450°C for 1 hour to sinter the $TiO_2$. After cooling, the $TiO_2$ photoanode was submerged in 10 mL of anthocyanin natural dye for 24 hours.

On the other hand, PVDF NF was soaked in an electrolyte solution for 1 hour. These electrolyte-treated membranes were then coated into a carbon-coated cathode FTO glass plate. Finally, the sandwich form of the DSSC-based FTO/-$TiO_2$/Acy/PVDF/C/FTO system was formed, completing the assembly of the DSSC. This fabrication is visualized in Figure 1.

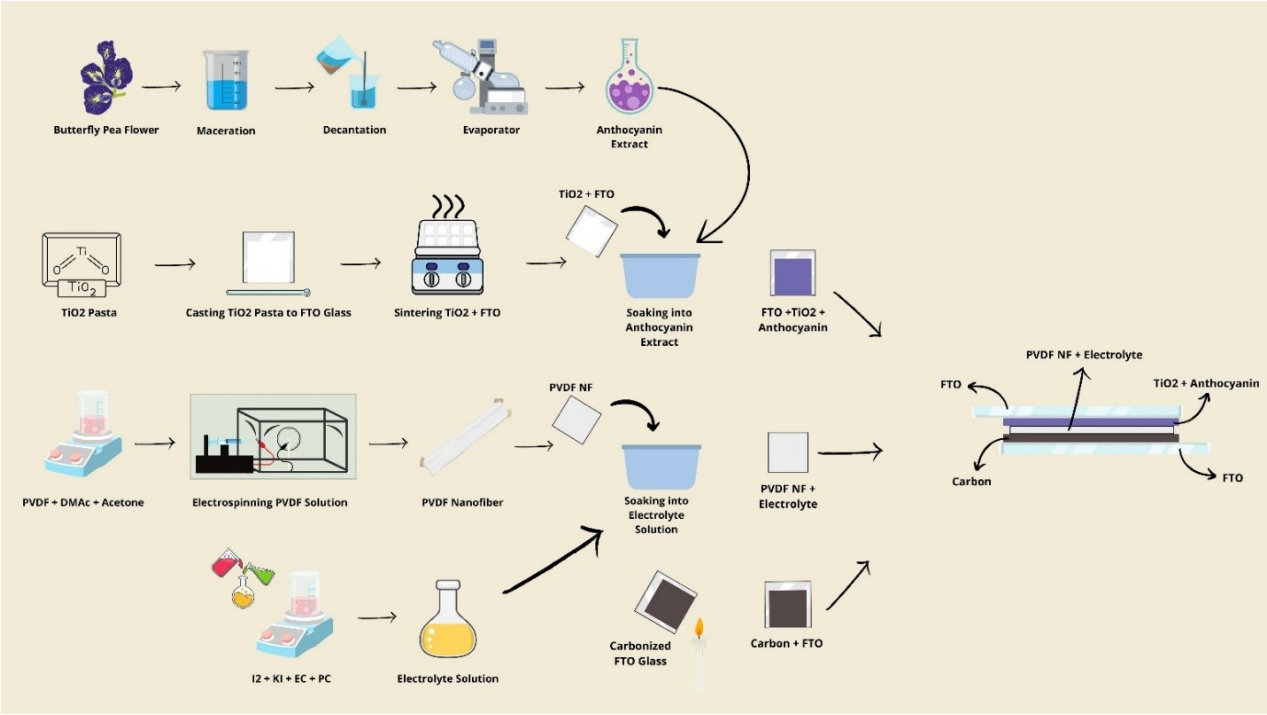


**Figure 1.** The Prototype of the DSSC Based FTO/$TiO_2$/Acy/PVDF/C/FTO Module Fabrication Route

Furthermore, 20 DSSC cells with optimal voltage and current are arranged in a module with a mixed circuit containing series and parallel circuits to measure electrical parameters including current and voltage through a multimeter. The DSSC module is irradiated with lamps and variations in the length of the irradiation time to obtain optimal current and voltage results on the DSSC module by analyzing its electrical parameters using a multimeter. The DSSC module with optimal voltage and current is installed with a module support device so that it can store current and voltage using a battery with variations in storage time, which will affect the amount of current and voltage stored in the battery.

## 3. RESULTS AND DISCUSSION

### 3.1 DSSC Characterization

The DSSC module fabrication process is illustrated in Figure 1, showing the systematic assembly of the FTO/$TiO_2$/Acy/PVDF-/C/FTO composite structure. To confirm the successful formation of this composite, multiple complementary characterization techniques were employed for each component. These comprehensive analytical techniques provide concrete evidence for the proper formation of each material component during the DSSC fabrication process, ensuring the successful integration of all layers in the final device structure.

### 3.2 UV Absorption

The dye in DSSC plays a crucial role in enhancing visible light absorption on $TiO_2$. Natural dyes offer several advantages over synthetic alternatives, including ready availability,

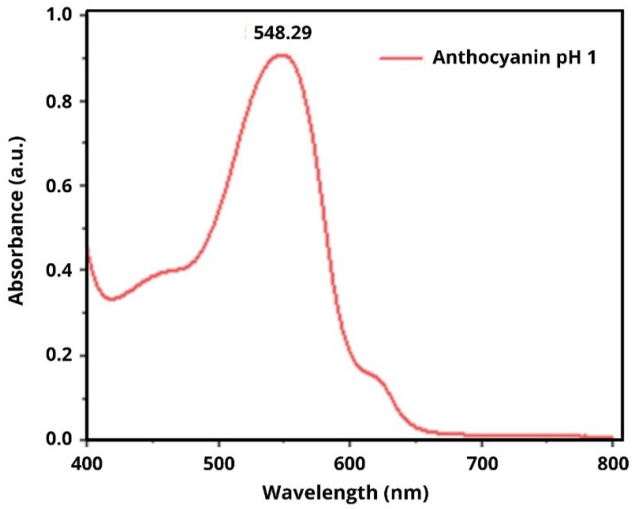


**Figure 2.** UV Absorption of Anthocyanin pH 1

simpler extraction processes, high absorption coefficients, cost-effectiveness, non-toxicity, and biodegradability. Butterfly pea (*Clitoria ternatea* L.) flower extract is particularly rich in anthocyanins. It exhibits a characteristic deep-blue color and remarkable stability in low-acidic solutions. This stability is attributed to the presence of polyacrylate anthocyanins, which undergo intramolecular co-pigmentation, preventing color degradation (Chandrajith et al., 2021). Various factors influence the

color stability of butterfly pea flowers, including pH, chemical structure, light exposure, and temperature (Marpaung and Pustikarini, 2023). The effectiveness of anthocyanins in DSSC applications is supported by carbonyl and hydroxyl groups in anthocyanins, which facilitate both color retention on $TiO_2$ surfaces and electron transfer from HOMO to LUMO states, subsequently enabling electron injection into the $TiO_2$ conduction band. To evaluate the potential of anthocyanin as a natural sensitizer in DSSC, UV-Vis spectrophotometric analysis was conducted across the visible spectrum (400-800 nm).

Figure 2 shows the UV-Vis spectral analysis of the butterfly pea flower extract at pH 1, this graph shows a prominent absorption peak at 548.29 nm, which matches previous findings reporting the resonance wavelength of anthocyanins to be around 550 nm (Marpaung and Pustikarini, 2023). The strong absorption characteristics can be attributed to the $\pi$-conjugated structure of anthocyanin, where greater conjugation corresponds to stronger coloration and higher absorption wavelengths. These pigment characteristics enable effective binding with $TiO_2$, potentially enhancing DSSC efficiency through improved energy conversion rates.

### 3.3 FTIR

The FTIR analysis of PVDF and PVDF-NF has been described in a previous study published in another journal by Kusumawati et al. (2023). The FTIR results show that PVDF-NF exhibits significant differences in its molecular structure and crystal phase, as shown in the spectra data in Figure 3. From the spectra, it can be concluded that the electrospinning process applied to make PVDF-NF resulted in a noticeable peak shift compared to pure PVDF, especially in the characteristic bands associated with $CF_2$ asymmetric stretching (shifted from 841.15 $cm^{-1}$ to 838.81 $cm^{-1}$) and combined $CF/CF_2$ stretching and $CH_2$ bending (shifted from 873.09 $cm^{-1}$ to 875.84 $cm^{-1}$). The addition of electrolytes to PVDF-NF seems to affect the polymer chain interactions, leading to less pronounced amorphous phase peaks. This suggests that the electrospinning process not only affects the physical structure but also modifies the molecular arrangement and crystallinity of the PVDF material, with the electrolyte further impacting the polymer-solvent interactions in the PVDF-NF system (Kusumawati et al., 2024). These molecular rearrangements, coupled with reduced amorphous phase peaks upon electrolyte addition, indicate enhanced polymer chain flexibility and improved electrolyte uptake capacity. Such structural modifications are particularly beneficial for DSSC applications, as they create an optimal framework for electrolyte retention. The more organized molecular structure and modified crystallinity of PVDF-NF provide better pathways for ion transport while maintaining sufficient mechanical stability to prevent electrolyte leakage (Almafie et al., 2024). This balanced combination of properties makes PVDF-NF membranes highly effective in maintaining stable electrolyte solutions within DSSC circuits, potentially leading to improved long-term cell performance and efficiency.

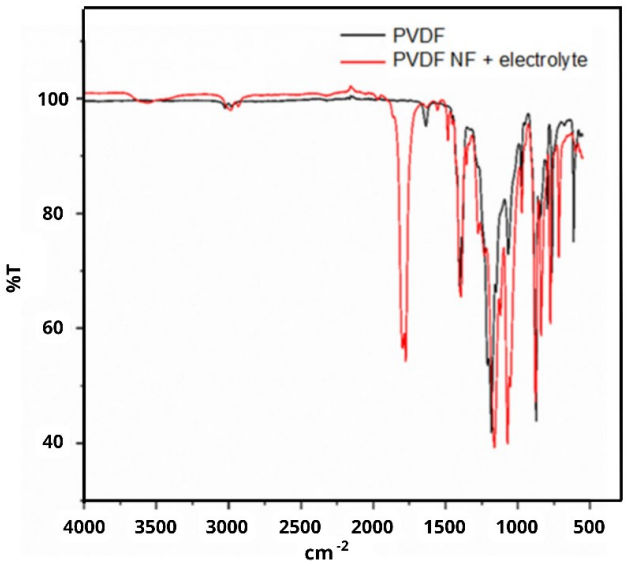


**Figure 3.** FTIR Peak Analysis of the Different PVDF and PVDF-NF (Kusumawati et al., 2023)

### 3.4 SEM

The fabricated PVDF-NF membrane is designed to trap electrolytes better than conventional PVDF membranes. In conventional PVDF membranes, the higher the level of particulate density, the greater the driving force to pass particulates through the membrane and the slower the speed of the electrolyte solution passing through the membrane, so that the electron flow rate in charge transport is slower, which can reduce the electrical efficiency value (Almafie et al., 2024; Kusumawati et al., 2024). As a solution, the fabrication of a PVDF-NF membrane by electrospinning technology shows a high membrane density to trap the electrolyte solution from excessive leakage, but enough to create a (path) so that the electron interaction is not disturbed with more efficient electron movement and capture. Thus, the electrical efficiency value of DSSC can be improved. SEM results of PVDF-NF have been revealed in previous research by Kusumawati et al. (2023) with 500× magnification for cross-section and 30.000× magnification for surface morphology shown in Figure 4.

Based on SEM analysis of the PVDF-NF membranes fabricated via electrospinning technology, some distinctive morphological features appeared that significantly improved the performance of DSSC. Cross-sectional images of Figures 4(a) and 4(b) show a well-developed finger-like macrovoid structure, creating a network of interconnected channels throughout the membrane thickness. This structural configuration proved essential for effective electrolyte retention in the DSSC system. Further examination of the surface morphology at higher magnification (30.000×), as shown in Figures 4(c) and 4(d), reveals the formation of randomly oriented nanofibers with uniform diameter distribution, forming a complex three-dimensional network with numerous interconnected pores.

**Table 1.** Voltametric Parameters of Anthocyanin Pigment (Kusumawati et al., 2024)

| Dyes | $E_{ox}$ (eV) | $E_{red}$ (eV) | Homo (eV) | Lumo (eV) | Band-gap (eV) |
|---|---|---|---|---|---|
| Anthocyanin | -0.1037 | -0.3489 | -4.2963 | -4.0511 | 0.2452 |

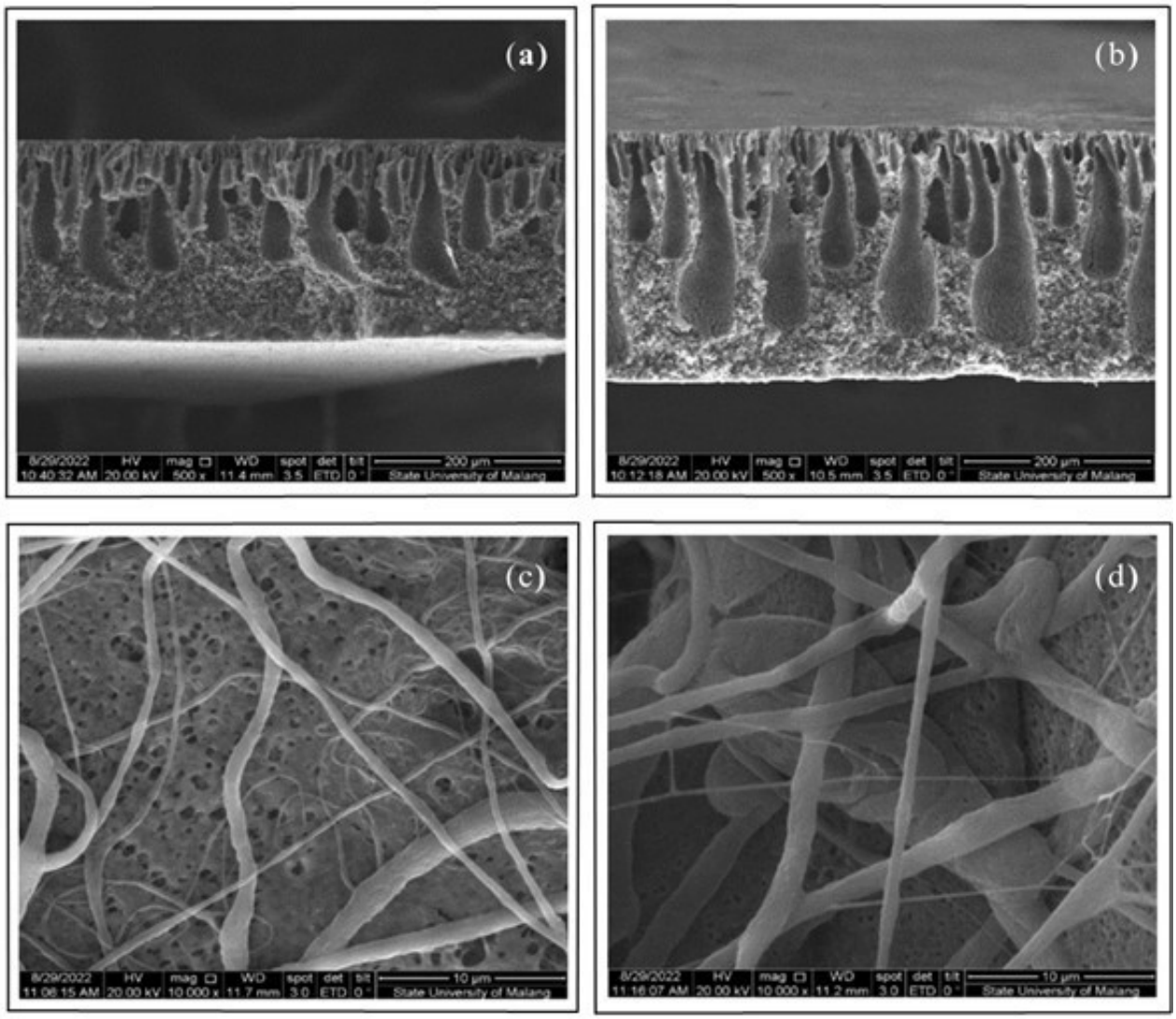


**Figure 4.** SEM Results of Polymer Electrolyte: Cross-section 500×; (a) PVDF 0.2 mm, (b) PVDF 0.6 mm, and Surface Morphology 30.000×; (c) PVDF-NF 0.35 mm, (d) PVDF NF 0.45 mm (Kusumawati et al., 2024)

This sophisticated architecture creates multiple nanoscale capillary channels that effectively trap the electrolyte solution through capillary action and surface tension effects, while the high surface area-to-volume ratio of the nanofibers enhances the interface between the membrane and electrolyte, thus promoting superior ionic conductivity (Nirwan et al., 2024). The hierarchical porosity system, which combines finger-like macrovoids and nanofibers surface structures, creates an optimal environment for electrolyte retention and ion transport (Cheng and Bae, 2024). Macro-scale retention occurs within the finger-like cavities, while micro-scale entrapment occurs within the nanofiber mesh, which collectively prevents electrolyte leakage through enhanced mechanical stability of the integrated structure. The interconnected network of pores, visible in both surface and cross-sectional views, provides an ideal pathway for ion movement while maintaining the physical containment of the electrolyte solution. These favorable morphological characteristics result in significantly improved electrolyte retention compared to conventional membranes, leading to improved long-term stability and higher efficiency

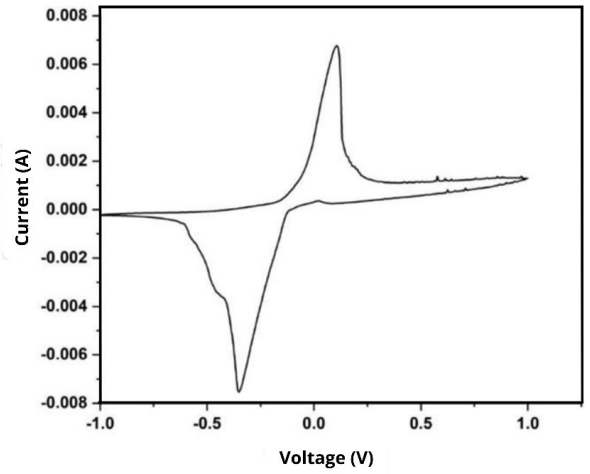


**Figure 5.** Cyclic Voltammetry Analysis Result of Anthocyanin Photosensitizer (Kusumawati et al., 2024)

potential in DSSC applications.

### 3.5 Cyclic Voltammetry Analysis

The cyclic voltammetry analysis in this study depends on our previous research findings by Kusumawati et al. (2024). The cyclic voltammetry analysis in Figure 5 and Table 1 revealed crucial insights into the electrochemical properties of this DSSC system.

Electrochemical analysis via voltammetric measurements showed high-efficiency electron transfer dynamics between dye bandgap energy and semiconductor energy, in which $TiO_2$ has 3.2 eV for anatase and 3.0 eV for the rutile phase (Kusumawati et al., 2024). These favorable electrochemical properties, coupled with the superior electrolyte retention ability of the PVDF NF membrane structure, significantly improved the overall performance of the DSSC. Voltammetric analysis of these anthocyanin pigments identified critical oxidation ($E_{ox}$) and reduction ($E_{red}$) potentials in Table 1 with values of $E_{ox}$ (-0.1037 eV) and $E_{red}$ (-0.3489 eV), which enabled precise calculations of Highest Occupied Molecular Orbital (HOMO), Lowest Occupied Molecular Orbital (LUMO), and band gap energies. The determination of the dye band gap energy follows the equation.

$$E_{HOMO} = -e(E_{ox} + 4.4)\ \text{eV} \quad (1)$$

$$E_{LUMO} = -e(E_{red} + 4.4)\ \text{eV} \quad (2)$$

$$E_g = E_{LUMO} - E_{HOMO} \quad (3)$$

These measurements show HOMO values at -4.2963 eV and LUMO values at -4.0511 eV, which verifies the compatibility of the dye as an effective photosensitizer with a bandgap value of 0.2452 eV, mainly due to the optimal alignment of LUMO with the conduction band of $TiO_2$, which facilitates efficient electron injection. These cyclic voltammetry results extend these initial findings, further validating the effectiveness of natural anthocyanin pigments in DSSC systems while demonstrating enhanced charge transport capabilities and stable electrolyte hold-up.

**Table 2.** Photovoltaic DSSC Analysis with Variations in the Length of Irradiation

| Time (h) | Voltage (mV) Irradiation | Current ($\mu$A) |
|---|---|---|
| 1 | 845 | $12.5 \times 10^{-3}$ |
| 2 | 1.050 | $15 \times 10^{-3}$ |
| 3 | 1.365 | $18 \times 10^{-3}$ |
| 4 | 1.625 | $20 \times 10^{-3}$ |
| 5 | 2.050 | $23.5 \times 10^{-3}$ |

### 3.6 Irradiation Time

In tropical countries such as Indonesia, which is crossed by the equator, sunlight is available throughout the year, thus providing the potential for environmentally friendly electrical energy through DSSC modules (Dambhare and Moharil, 2023; Estiningtyas et al., 2023).

The FTO/$TiO_2$/Acy/PVDF/C/FTO-based sandwich DSSC was fabricated in stages as shown in Figure 1, then assembled into modules consisting of 20 pairs arranged in parallel. The use of DSSC modules to produce electricity is mounted facing one particular direction. The sun's daily apparent motion leads it to change position every day, resulting in a varied intensity of sunlight at each hour. Thus, the position of the DSSC module greatly affects the intensity of the light obtained. Li et al. (2021) note that reduced sunlight leads to fewer photons reaching the module, subsequently decreasing the number of released electrons and lowering the output current at all voltages because of the decrease in light intensity. The number of photons per second that penetrates the cell will also decrease so that the number of electrons released is also reduced (Li et al., 2021).

Based on Table 2 and Figure 6(a) examined in this context, the duration of irradiation affects the parameter values of voltage and current of the DSSC circuit. For 1 hour of irradiation, it produces a voltage value of 845 mV, after 2 hours, it produces a voltage value of 1.050 mV, while 3 and 4 hours produce 1.365 and 1.625 mV. The longest irradiation for 5 hours produces 2.050 mV. The longer the irradiation time, the more the intensity of light absorbed, and the more the number of photos per second that penetrate the cell will be so that more electrons are released. With the number of electrons released, the voltage value of a DSSC module will increase.

Meanwhile, in Table 2, photovoltaic DSSC analysis with variations in the length of irradiation and Figure 6(b), the effect of irradiation time on the current value of the DSSC circuit

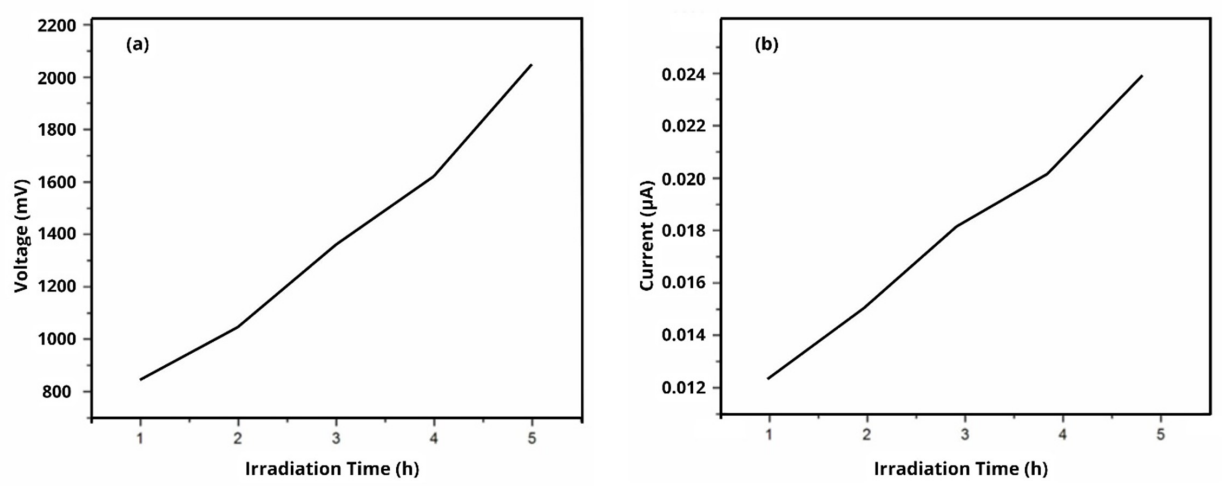


**Figure 6.** The Effect of Irradiation Time on (a) the Voltage Value and (b) the Value of the Electric Current of the DSSC circuit

above, the duration of irradiation affects the parameter values of voltage and current of the DSSC circuit. For 1 hour of irradiation, it produces a voltage value of $12.5 \times 10^{-3}$ $\mu$A, after 2 hours, it produces a voltage value of $15 \times 10^{-3}$ $\mu$A while 3 and 4 hours produce $18 \times 10^{-3}$ and $20 \times 10^{-3}$ $\mu$A. The longest irradiation for 5 hours produces $23.5 \times 10^{-3}$ $\mu$A. The longer the irradiation time, the more the intensity of light absorbed, and the more the number of photos per second that penetrate the cell will be so that more electrons are released. With the number of electrons released, the current value of a DSSC module will increase.

The length of irradiation time affects the value of light intensity and electrical efficiency, as shown in Figures 6(a) and 6(b). The longer the irradiation on the DSSC module, the greater the light intensity obtained. The relationship between light intensity and the quantum yield of photon-to-current conversion is fundamental in the operation of DSSC. An increase in incident light intensity results in a greater influx of photons, which directly correlates with an increase in generated current. Consequently, as both light intensity and the resulting current rise, there is an enhancement in the voltage output. This interdependence suggests that higher light intensity not only boosts current generation but also optimizes the electrical efficiency of the DSSC module, leading to improved overall performance in energy conversion.

### 3.7 Electrical Current Storage Time

Current storage is the capture of the current generated at one time for use at a later time to reduce the imbalance between current demand and current production in electrical energy (Colbertaldo et al., 2019). Accumulators, or batteries, are generally described as devices that store electrical current by converting electrical energy from chemical energy. It principally converts a form that is difficult to store to a form that is easier to store or save economically (Fagiolari et al., 2022; Raj et al., 2021). In batteries, electrons move from the electrodes to another substance through an external circuit, facilitating chemical reactions (Guo et al., 2023). This electron flow generates an electric current that can be harnessed for various tasks. During the operation of a power supply, the cathode serves as the positive terminal, while the anode functions as the negative terminal (Kadier et al., 2023). Upon connecting a battery to an external electrical load, a redox reaction takes place, wherein high-energy reactants are transformed into lower-energy products. This process results in a measurable difference in Gibbs energy, which is subsequently conveyed to the external circuit in the form of electrical energy (Eapen et al., 2021).

Batteries discharge direct current (DC), not alternating current, from their sockets. In a DC system, electrical charge is capable of flowing in only one direction (Hoenicke et al., 2021). Conversely, in an alternating current (AC) system, charges continuously oscillate, moving back and forth and constantly changing their direction (Chen et al., 2020).

Current refers to the flow of electric charge, which occurs due to a difference in electrical potential (Xiao et al., 2019). For current to flow, a complete circuit is necessary to allow the charge to return to its initial position. The magnitude of current (I) is measured in Amperes (A) or Coulombs per second (C/s), indicating the amount of charge (q) passing through a point per second. This relationship can be expressed using the following Equation 4 (Folkestad et al., 2020).

$$I = \frac{q}{t} \tag{4}$$

Electrons are the moving charges responsible for current through the wires in an electrical circuit (Blum, 2022). When a battery creates a potential difference, it generates an electric field that influences electron movement (Chang et al., 2020).

**Table 3.** The Effect of Irradiation Time on the Value of the Electric Current of the DSSC Circuit

| Day | Initial Current (μA) | Storage Time (hour) DSSC Current (μA) | | | | | Battery Current (μA) | | | | |
|---|---|---|---|---|---|---|---|---|---|---|---|
| | | 2 | 3 | 4 | 5 | 6 | 2 | 3 | 4 | 5 | 6 |
| 1 | | 11.9 | 11.8 | 11.75 | 11.6 | 11.55 | 0.1 | 0.2 | 0.25 | 0.4 | 0.45 |
| 2 | | 10.4 | 10.15 | 10.10 | 10.0 | 9.7 | 0.6 | 0.85 | 0.9 | 1.0 | 1.3 |
| 3 | | 9.5 | 9.4 | 7.15 | 7.10 | 7.9 | 6.5 | 1.6 | 1.85 | 1.90 | 2.1 |
| 4 | 12 μA | 6.7 | 5.9 | 5.0 | 4.1 | 3.7 | 4.3 | 4.6 | 5.0 | 5.9 | 6.3 |
| 5 | | 3.5 | 3.1 | 2.45 | 2.25 | 2.15 | 6.5 | 6.9 | 7.55 | 7.75 | 8.85 |
| 6 | | 1 | 0.5 | 0.48 | 0 | 0 | 9.0 | 10.5 | 11.52 | 12.0 | 12.0 |
| 7 | | 0 | 0 | 0 | 0 | 0 | 12.0 | 12.0 | 12.0 | 12.0 | 12.0 |
| 8 | | 0 | 0 | 0 | 0 | 0 | 12.0 | 12.0 | 12.0 | 12.0 | 12.0 |

While electrons move randomly even without an electric field, the presence of a field produces a slight overall movement known as drift velocity, which opposes the electric field due to the negative charge of the electrons (Folkestad et al., 2020; Anwar et al., 2022).

Voltage acts as the driving force for electric charge in a conductor, but resistance affects how easily the charge can flow (Chang et al., 2020). Resistance (R) is determined by the conductor's length, cross-sectional area, and resistivity (r), expressed mathematically in Equation 5 (Becker et al., 2022).

$$R = \rho \frac{L}{A} \tag{5}$$

Resistance and conductivity exhibit an inverse relationship; materials characterized as good conductors possess low resistance, whereas insulators are defined by high resistivity (Han et al., 2021). Additionally, resistance is generally temperature-dependent. As a result, resistance increases with temperature changes, as described by specific equations in Equation 6 and Equation 7 (Shenogin et al., 2020).

$$\rho = \rho_0[1 + \alpha(T - T_0)] \tag{6}$$

$$R = R_0[1 + \alpha(T - T_0)] \tag{7}$$

When subjected to low temperatures, certain materials known as superconductors exhibit zero resistance (Revathy et al., 2021). On the other hand, the presence of resistance in cables leads to energy dissipation, typically in the form of heat (Li et al., 2020). To store current in the battery, the DSSC was assembled to generate current in a module and studied for 8 days to check the most efficient storage time and reproducibility (Khir et al., 2022). Therefore, the temporal efficiency progress for 2 hours of the DSSC module was investigated, and the results are obtained in Table 3 current measurements at

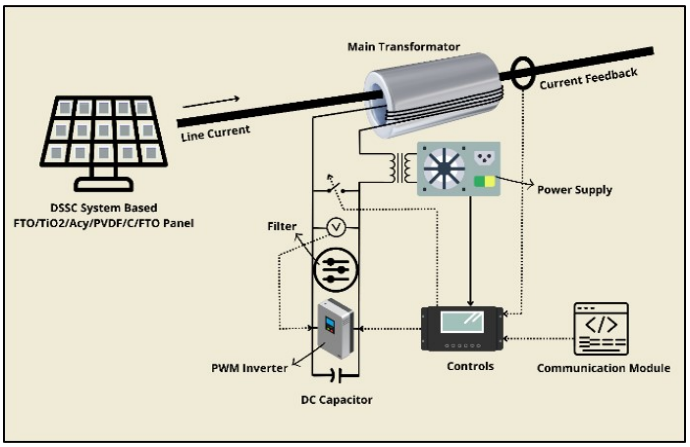


**Figure 7.** The Circuit Module Saves Energy from DSSC to the Power Supply

predetermined hours and days give the results of a significant decrease in current after 4 days. The current value gradually decreases as the current continues to flow to the battery. Thus, it increases the current of the battery (Akcaoglu et al., 2019; Zhang et al., 2019; Mejica et al., 2022; Nam and Boo, 2022).

Table 3 presents a detailed analysis of the effects of irradiation and storage duration on the current characteristics of DSSC. An increase in storage time correlates with a decrease in current values across all initial ranges, from 0 μA to 12 μA. Conversely, the battery charge factor exhibits an upward trend, increasing from 0 μA to 12 μA after the cell has remained idle for one hour. Notably, the open-circuit photovoltage remains invariant, reflecting the stable potential difference between the $TiO_2$ energy level and the redox potential of the PVDF electrolyte (Yoo et al., 2019).

The observed decline in current can be attributed to several interrelated factors. These include the photodegradation of dye molecules, which reduces their efficiency; alterations in the dynamics of light reflection; fouling of the PVDF semiconductor material; and degradation of the electrolyte. Collectively,

**Table 4.** Comparison of Photoelectrochemical Performance with Similar Materials Reported in the Literature

| Dye photosensitizer | Efficiency (%) | Electrolyte | References |
|---|---|---|---|
| Butterfly pea flower (Anthocyanin) | 2.4 | 9.2 mg I2, 0.06 g KI, 0.4 g EC, and 0.4 g PC in PVDF NF Membrane | (Kusumawati et al., 2024) |
| Pandan leaves *P.amaryllifolius* (Chlorophyll) | 0.1 | 0.5 M KI; 0.05 M I dissolved in the solution of ethylene glycol and acetonitrile at a volume ratio of 4:1 | (Al-Alwani et al., 2017) |
| Leaves of *Acacia nilotica* (Chlorophyll) | 0.5-0.7 | 0.67 g of lithium iodide, 0.13 g of iodine, and 10 ml of acetonitrile | (Dhanasekaran and Marimuthu, 2022) |
| Cocktail dye of *Hibiscus sabdariffa* (Anthocyanins), *Beta vulgaris* (Betalains), and *Spinacia oleracea* (Chlorophyll) | 3.7 | Liquid electrolyte | (Patni et al., 2020) |
| Beetroot (Betanine) | 1.3 | Liquid electrolyte | (Sathyajothi et al., 2017) |
| Ag NP/multi-branched $TiO_2$ | 10.0 | LiI + $I_2$ + DMII + TBP | (Chen et al., 2019) |
| Sensitized dye (N719) - Ru(II)-complex | 0.6 | Aqueous I-/I-3 electrolyte | (Ibrahim et al., 2021) |

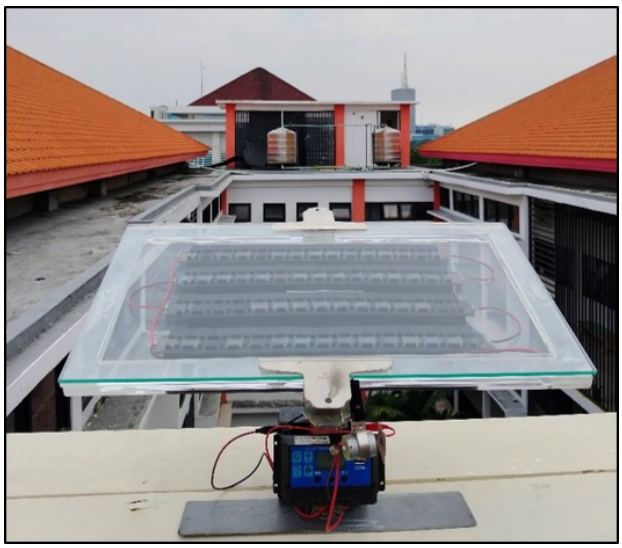

**Figure 8.** The Prototype of the DSSC Module

these phenomena lead to a significant decrease in the overall efficiency of the photovoltaic system (Belessiotis et al., 2022).

In contrast, the current measured in the connected battery which reflects the quantity of charge stored—increases with prolonged storage time. This inverse correlation occurs because, as the efficiency of the DSSC diminishes, a larger fraction of the generated charge is sequestered within the battery. This phenomenon can be elucidated through an analysis of variations in series resistance within the equivalent circuit of the DSSC module (Tayeb et al., 2022).

These findings emphasize the long-term stability and reliability of DSSC, which is crucial for their implementation in solar energy conversion and storage systems. Furthermore, by injecting and measuring the electrolyte initially, it is possible to determine the electrical characteristics of the DSSC over a period, providing valuable insights into its operational behavior and performance dynamics.

The circuit module to save energy from DSSC to the power supply is depicted in Figure 7 which is implemented on a real DSSC module prototype in Figure 8. It bridges the main transformer, controller, Pulse Width Modulation (PWM) inverter, power supply, DC capacitor, and communication module. The main transformer is directly connected to and suspended from the transmission line, whereas the line conductor acts as a secondary winding. PWM inverter technologies regulate the inverter output voltage in quadrature with the grid current, utilizing the features of Insulated Gate Bipolar Transistors (IGBTs), Line Current (LC) filters, and DC capacitors to generate grid power. A communication module integrated with wireless technologies or power line communication for real-time adjustment. Additionally, a feedback current transformer provides essential control power when the mains current exceeds established limits, thereby enhancing grid stability and power quality (Iwata et al., 2018; Venkateswari and Sreejith, 2019; Mendizabal et al., 2022; Nasrollahi et al., 2022). For a comparison of efficiency in this module, we are shown the comparison table of our DSSC module efficiency versus another research in Table 4.

Our DSSC fabrication demonstrated superior performance with an efficiency of 2.4%, which surpasses other single pigment dyes such as chlorophyll (ranging from 0.1-0.6%) and betanin (1.3%). Although the efficiency remains below that of metal-based photosensitizers, the natural dyes employed in this study prioritize eco-friendliness and long-term sustainability.

Furthermore, while the PVDF NF-based electrolyte exhibits comparable efficiency to liquid electrolytes, the polymer-based electrolyte system offers enhanced storage stability by minimizing electrolyte leakage through the entrapment of the electrolyte solution within the PVDF NF membrane (Kusumawati et al., 2024).

## 4. CONCLUSIONS

Enhancing the efficiency of DSSC modules can be accomplished through a variety of methods. A particularly effective strategy involves the irradiation of the module with light for defined intervals. Experimental data indicate that an optimal irradiation time of 5 hours enables the module to generate 2.050 mV and $23.5 \times 10^{-3}$ $\mu$A. As the irradiation duration is extended, there is a corresponding increase in light absorption by the cell, resulting in an elevated rate of photon penetration. This augmentation in phot-on influx leads to a greater release of electrons, thereby enhancing the current output across all voltage levels of the module. It is important to note that the current generated by the module remains relatively modest, necessitating its subsequent storage in a battery system. Analyses reveal that effective current storage within the DSSC module circuit is achieved by the $8^{th}$ day of operation, following 6 hours of irradiation, yielding a current of 12 $\mu$A that flows into the battery. As the duration of battery storage increases, a greater quantity of current can be accumulated. Moreover, the rate at which the battery charges is directly influenced by the electrical efficiency of the system; a higher electrical efficiency correlates with a more rapid attainment of full charge within the battery. Thus, optimizing the operational parameters of the DSSC module is crucial for maximizing current output and enhancing energy storage capabilities.

## 5. ACKNOWLEDGEMENT

We gratefully acknowledge the Ministry of Education and Culture, Research and Technology of the Republic of Indonesia for their financial support. We also thank the Department of Chemistry, Faculty of Mathematics and Natural Sciences, Universitas Negeri Surabaya for providing laboratory facilities and the 'Merah Putih' research team for their assistance and motivation.

## REFERENCES

Agrawal, A., S. A. Siddiqui, A. Soni, K. Khandelwal, and G. D. Sharma (2021). Performance Analysis of $TiO_2$ Based Dye Sensitized Solar Cell Prepared by Screen Printing and Doctor Blade Deposition Techniques. *Solar Energy*, **226**; 9–19

Akcaoglu, S. C., G. Martinopoulos, C. Koidis, D. Kiymaz, and C. Zafer (2019). Investigation of Cell-Level Potential-Induced Degradation Mechanisms on Perovskite, Dye-Sensitized and Organic Photovoltaics. *Solar Energy*, **190**; 301–318

Al-Alwani, M. A. M., A. B. Mohamad, A. A. H. Kadhum, N. A. Ludin, N. E. Safie, M. Z. Razali, M. Ismail, and K. Sopian (2017). Natural Dye Extracted from *Pandanus amaryllifolius* Leaves as Sensitizer in Fabrication of Dye-Sensitized Solar Cells. *International Journal of Electrochemical Science*, **12**(1); 747–761

Ali, M., E. Pervaiz, U. Sikandar, and Y. Khan (2021). A Review on the Recent Developments in Zirconium and Carbon-Based Catalysts for Photoelectrochemical Water-Splitting. *International Journal of Hydrogen Energy*, **46**(35); 18257–18283

Almafie, M. R., R. Dani, R. Riyanto, L. Marlina, J. Jauhari, and I. Sriyanti (2024). Preparation of PAN/PVDF Nanofiber Mats Loaded with Coconut Shell Activated Carbon and $SiO_2$ for Lithium-Ion Battery Anodes. *Science and Technology Indonesia*, **9**(2); 427–447

Amir-Al Zumahi, S. M., N. Arobi, M. Mahbubur Rahman, M. Kamal Hossain, M. Ara Jahan Rozy, M. S. Bashar, A. Amri, H. Kabir, M. Abul Hossain, and F. Ahmed (2021). Understanding the Optical Behaviours and the Power Conversion Efficiency of Novel Organic Dye and Nanostructured $TiO_2$ Based Integrated DSSCs. *Solar Energy*, **225**; 129–147

Andualem, A. and S. Demiss (2018). Review on Dye-Sensitized Solar Cells (DSSCs). *Edelweiss Applied Science and Technology*, **2**(1); 145–150

Anwar, O., A. Keating, R. Cardell-Oliver, A. Datta, and G. Putrino (2022). Design and Development of Low-Power, Long-Range Data Acquisition System for Beehives - BeeDAS. *Computers and Electronics in Agriculture*, **201**; 107281

Bandara, T. M. W. J., A. M. J. S. Weerasinghe, M. A. K. L. Dissanayake, G. K. R. Senadeera, M. Furlani, I. Albinsson, and B. E. Mellander (2018). Characterization of Poly (Vinylidene Fluoride-Co-Hexafluoropropylene) (PVdF-HFP) Nanofiber Membrane Based Quasi Solid Electrolytes and Their Application in a Dye Sensitized Solar Cell. *Electrochimica Acta*, **266**; 276–283

Becker, S., M. Michel, P. Mitschang, and M. Duhovic (2022). Influence of Polymer Matrix on the Induction Heating Behavior of CFRPC Laminates. *Composites Part B: Engineering*, **231**; 109561

Belessiotis, G. V., I. Ibrahim, and P. Falaras (2022). Sensitizer Effects on DSSC Performance Under Pan-Illumination Conditions. *Journal of Photochemistry and Photobiology A: Chemistry*, **433**; 114201

Blum, M. (2022). *An Inquiry-Based Introduction to Engineering*. Springer International Publishing

Cakar, S. (2019). 1,10 Phenanthroline 5,6 Diol Metal Complex (Cu, Fe) Sensitized Solar Cells: A Cocktail Dye Effect. *Journal of Power Sources*, **435**; 226825

Chandrajith, G., V. Gamage, Y. Y. Lim, and W. S. Choo (2021). Anthocyanins From *Clitoria ternatea* Flower: Biosynthesis, Extraction, Stability, Antioxidant Activity, and Applications. *Frontiers in Plant Science*, **12**; 792303

Chang, J., S. Zang, Y. Wang, C. Chen, D. Wu, F. Xu, and Z. Gao (2020). $Co_3O_4$@$Ni_3S_4$ Heterostructure Composite Constructed by Low Dimensional Components as Efficient Battery Electrode for Hybrid Supercapacitor. *Electrochimica*

 

*Acta*, **353**; 136501
Chen, R., J. Bao, Z. Yan, X. Huang, J. Yun, X. Zeng, and J. Chen (2019). Preparation of Transparent Dispersions With Monodispersed Ag Nanoparticles for $TiO_2$ Photoelectrode Materials With Excellent Photovoltaic Performance. *Engineered Science*, **8**(6); 54–65
Chen, X. (2022). *Multifunctional Metal-Free Carbon Nanomaterials for Clean Energy Conversion and Storage Applications*. Ph.D. thesis, Case Western Reserve University
Chen, X., L. Gao, J. Chen, S. Lu, H. Zhou, T. Wang, and Y. Yang (2020). A Chaotic Pendulum Triboelectric-Electromagnetic Hybridized Nanogenerator for Wave Energy Scavenging and Self-Powered Wireless Sensing System. *Nano Energy*, **69**; 104440
Cheng, X. and J. Bae (2024). Recent Advancements in Fabrication, Separation, and Purification of Hierarchically Porous Polymer Membranes and Their Applications in Next-Generation Electrochemical Energy Storage Devices. *Polymers*, **16**(23); 3269
Colbertaldo, P., S. B. Agustin, S. Campanari, and J. Brouwer (2019). Impact of Hydrogen Energy Storage on California Electric Power System: Towards 100% Renewable Electricity. *International Journal of Hydrogen Energy*, **44**(19); 9558–9576
Dambhare, M. V. and S. V. Moharil (2023). A Systematic Review on Enhancing Efficiency of Solar Cells Using Upconversion. *Materials Today: Proceedings*, **92**; 865–870
Dhanasekaran, P. and R. Marimuthu (2022). Simultaneous Effect of Activated Carbon and Chlorophyll Pigment from Leaves of *Acacia nilotica* on the Enhancement of Electron Transfer in DSSC Applications. *Materials Research Express*, **9**(11); 116201
Dhorkule, M. R., P. Y. Lamrood, S. D. Ralegankar, S. P. Patole, S. S. Wagh, and H. M. Pathan (2024). Unveiling the Efficiency of Dye-Sensitized Solar Cells: A Journey from Synthetic to Natural Dyes. *ES Food and Agroforestry*, **16**; 1–21
Eapen, D. E., R. Suresh, S. Patil, and R. Rengaswamy (2021). A Systems Engineering Perspective on Electrochemical Energy Technologies and a Framework for Application Driven Choice of Technology. *Renewable and Sustainable Energy Reviews*, **147**; 111165
Erande, K. B., P. Y. Hawaldar, S. R. Suryawanshi, B. M. Babar, A. A. Mohite, H. D. Shelke, and U. T. Pawar (2021). Extraction of Natural Dye (Specifically Anthocyanin) from Pomegranate Fruit Source and Their Subsequent Use in DSSC. *Materials Today: Proceedings*, **43**; 2716–2720
Estiningtyas, I. W., N. Kusumawati, P. Setiarso, S. Muslim, N. T. Rahayu, R. N. Safitri, and F. F. Fachrirakarsie (2023). Effect of Natural Dye Combination and pH Extraction on the Performance of Dye-Sensitized Photovoltaics Solar Cell. *International Journal of Renewable Energy Development*, **12**(6); 1054–1060
Fagiolari, L., M. Sampò, A. Lamberti, J. Amici, C. Francia, S. Bodoardo, and F. Bella (2022). Integrated Energy Conversion and Storage Devices: Interfacing Solar Cells, Batteries and Supercapacitors. *Energy Storage Materials*, **51**; 400–434
Farghali, M., A. I. Osman, I. M. A. Mohamed, Z. Chen, L. Chen, I. Ihara, P. S. Yap, and D. W. Rooney (2023). Strategies to Save Energy in the Context of the Energy Crisis: A Review. *Environmental Chemistry Letters*, **21**(4); 2003–2039
Fetouh, H. A., A. E. Dissouky, H. A. Salem, M. Fathy, B. Anis, and A. E. H. Kashyout (2024). Synthesis, Characterization and Evaluation of New Alternative Ruthenium Complex for Dye Sensitized Solar Cells. *Scientific Reports*, **14**(1); 1–13
Folkestad, C. A., N. Hansen, K. Fagerholt, H. Andersson, and G. Pantuso (2020). Optimal Charging and Repositioning of Electric Vehicles in a Free-Floating Carsharing System. *Computers & Operations Research*, **113**; 104771
Guo, T., P. Hu, L. Li, Z. Wang, and L. Guo (2023). Amorphous Materials Emerging as Prospective Electrodes for Electrochemical Energy Storage and Conversion. *Chem*, **9**(5); 1080–1093
Han, Y., X. Shi, S. Wang, K. Ruan, C. Lu, Y. Guo, and J. Gu (2021). Nest-Like Hetero-Structured BNNS@SiCnws Fillers and Significant Improvement on Thermal Conductivities of Epoxy Composites. *Composites Part B: Engineering*, **210**; 108666
Hoenicke, P., D. Ghosh, A. Muhandes, S. Bhattacharya, C. Bauer, J. Kallo, and C. Willich (2021). Power Management Control and Delivery Module for a Hybrid Electric Aircraft Using Fuel Cell and Battery. *Energy Conversion and Management*, **244**; 114445
Holechek, J. L., H. M. E. Geli, M. N. Sawalhah, and R. Valdez (2022). A Global Assessment: Can Renewable Energy Replace Fossil Fuels by 2050? *Sustainability (Switzerland)*, **14**(8); 1–22
Hosseinnezhad, M., K. Gharanjig, M. K. Yazdi, P. Zarrintaj, S. Moradian, M. R. Saeb, and F. J. Stadler (2020). Dye-Sensitized Solar Cells Based on Natural Photosensitizers: A Green View from Iran. *Journal of Alloys and Compounds*, **828**; 154329
Ibrahim, I., H. N. Lim, N. W. K. Wan, N. M. Huang, S. P. Lim, W. Busayaporn, and H. Nakajima (2021). Plasmonic Silver Sandwich Structured Photoanode and Reflective Counter Electrode Enhancing Power Conversion Efficiency of Dye-Sensitized Solar Cell. *Solar Energy*, **215**; 403–409
Iwata, S., S.-I. Shibakawa, N. Imawaka, and K. Yoshino (2018). Stability of the Current Characteristics of Dye-Sensitized Solar Cells in the Second Quadrant of the Current–Voltage Characteristics. *Energy Reports*, **4**; 8–12
Jalomo-Cuevas, J., F. C. Fonseca, J. Cárcel-Carrasco, S. S. Pérez, and A. Gudiño-Ochoa (2023). Impact of Solar Radiation on Luminaires and Energy Efficiency in Isolated Residential Photovoltaic Systems. *Buildings*, **13**(10); 1–17
Jensen, L. (2023). *Global Decarbonization in Fossil Fuel Export-Dependent Economies*. United Nations Development Programme
Kadier, A., R. Singh, D. Song, F. Ghanbari, N. S. Zaidi, P. T. P. Aryanti, and P.-C. Ma (2023). A Novel Pico-Hydro Power

 

(PHP)-Microbial Electrolysis Cell (MEC) Coupled System for Sustainable Hydrogen Production During Palm Oil Mill Effluent (POME) Wastewater Treatment. *International Journal of Hydrogen Energy*, **48**(55); 21066–21087

Khir, H., A. K. Pandey, R. Saidur, M. S. Ahmad, N. A. Rahim, M. Dewika, and M. Samykano (2022). Recent Advancements and Challenges in Flexible Low Temperature Dye Sensitised Solar Cells. *Sustainable Energy Technologies and Assessments*, **53**; 102745

Kula, S., A. Szlapa-Kula, A. Fabiańczyk, P. Gnida, M. Libera, K. Bujak, M. Siwy, and E. Schab-Balcerzak (2019). Effect of Thienyl Units in Cyanoacrylic Acid Derivatives Toward Dye-Sensitized Solar Cells. *Journal of Photochemistry and Photobiology B: Biology*, **197**; 111555

Kumar, Y., T. Chhalodia, P. K. G. Bedi, and P. Meena (2023). Photoanode Modified with Nanostructures for Efficiency Enhancement in DSSC: A Review. *Carbon Letters*, **33**(1); 35–58

Kusumawati, N., P. Setiarso, and S. Muslim (2018a). Polysulfone/Polyvinylidene Fluoride Composite Membrane: Effect of Coating Dope Composition on Membrane Characteristics and Performance. *Rasayan Journal Chemistry*, **11**(3); 1034–1041

Kusumawati, N., P. Setiarso, S. Muslim, Q. A. Hafidha, S. A. Cahyani, and F. F. Fachrirakarsie (2024). Optimization Thickness of Photoanode Layer and Membrane as Electrolyte Trapping Medium for Improvement Dye-Sensitized Solar Cell Performance. *Science and Technology Indonesia*, **9**(1); 7–16

Kusumawati, N., P. Setiarso, A. B. Santoso, S. Muslim, Q. A'yun, and M. M. Putri (2023). Characterization of Poly (Vinylidene Fuoride) Nanofiber-Based Electrolyte and its Application to Dye-Sensitized Solar Cell with Natural Dyes. *Indonesian Journal of Chemistry*, **23**(1); 113–126

Kusumawati, N., P. Setiarso, M. M. Sianita, and S. Muslim (2018b). Transport Properties, Mechanical Behavior, Thermal and Rhemical Resistance of Asymmetric Flat Sheet Membrane Prepared from PSf/PVDF Blended Membrane on Gauze Supporting Layer. *Indonesian Journal of Chemistry*, **18**(2); 257–264

Li, T., X.-Z. Yuan, L. Zhang, D. Song, K. Shi, and C. Bock (2020). Degradation Mechanisms and Mitigation Strategies of Nickel-rRch NMC-Based Lithium-ion Batteries. *Electrochemical Energy Reviews*, **3**(1); 43–80

Li, Z., J. Yang, and P. A. N. Dezfuli (2021). Study on the Influence of Light Intensity on the Performance of Solar Cell. *International Journal of Photoenergy*, **2021**; 1–10

Marpaung, A. M. and D. Pustikarini (2023). Spectrophotometric Change of Butterfly Pea (*Clitoria ternatea* L.) Flower Extract in Various Metal Ion Solutions During Storage. *Science and Technology Indonesia*, **8**(3); 367–372

Mauri, L., A. Colombo, C. Dragonetti, D. Roberto, and F. Fagnani (2021). Recent Investigations on Thiocyanate-Free Ruthenium (II) 2, 2-Bipyridyl Complexes for Dye-Sensitized Solar Cells. *Molecules*, **26**(24); 7638

Mejica, G. F. C., Y. Unpaprom, D. Balakrishnan, N. Dussadee, S. Buochareon, and R. Ramaraj (2022). Anthocyanin Pigment-Based Dye-Sensitized Solar Cells with Improved pH-Dependent Photovoltaic Properties. *Sustainable Energy Technologies and Assessments*, **51**; 101971

Mendizabal, J. K., M. Montazeri, D. Huitink, and N. Miljkovic (2022). Direct Cooling of a Planar Magnetic Converter using Dielectric Liquid Forced Convection Enabled by Additive Manufacturing. *International Journal of Heat and Mass Transfer*, **191**; 122809

Miettunen, K. and A. Santasalo-Aarnio (2021). Eco-Design for Dye Solar Cells: From Hazardous Waste to Profitable Recovery. *Journal of Cleaner Production*, **320**; 128743

Nam, S.-H. and J.-H. Boo (2022). Fabrication of Moth-eye Patterned $TiO_2$ Active Layers for High Energy Efficiency and Current Density of Dye-Sensitized Solar Cells. *Energy Reports*, **8**; 98–105

Narudin, N., P. Ekanayake, Y. W. Soon, H. Nakajima, and C. M. Lim (2021). Enhanced Properties of Low-Cost Carbon Black-Graphite Counter Electrode in DSSC by Incorporating Binders. *Solar Energy*, **225**; 237–244

Nasrollahi, R., H. F. Farahani, M. Asadi, and M. Farhadi-Kangarlu (2022). Sliding Mode Control of a Dynamic Voltage Restorer Based on PWM AC Chopper in Three-Phase Three-Wire Systems. *International Journal of Electrical Power & Energy Systems*, **134**; 107480

Nirwan, V. P., A. Amarjargal, R. Hengsbach, and A. Fahmi (2024). Electrospun Smart Hybrid Nanofibers for Multifaceted Applications. *Macromolecular Rapid Communications*; 2400617

Ozaydin, C. and M. Gozel (2023). The Use of Copper-Quercetin Complex as Photosensitizer in Dye Sensitive Solar Cells and Its Photovoltaic Performance. *Brazilian Journal of Physics*, **53**(1); 1–10

Patni, N., S. G. Pillai, and P. Sharma (2020). Effect of using Betalain, Anthocyanin and Chlorophyll Dyes Together as a Sensitizer on Enhancing the Efficiency of Dye-Sensitized Solar Cell. *International Journal of Energy Research*, **44**(13); 10846–10859

Raj, R., R. Verma, and J. Singh (2021). Nanomaterials for Energy Storage Applications. In *Clean Energy Production Technologies*. Springer Singapore, pages 135–156

Revathy, G., V. Rajendran, and P. S. Kumar (2021). Prediction Study on Critical Temperature (C) of Different Atomic Numbers Superconductors (Both Gaseous/Solid Elements) using Machine Learning Techniques. *Materials Today: Proceedings*, **44**; 3627–3632

Santamouris, M. and K. Vasilakopoulou (2021). Present and Future Energy Consumption of Buildings: Challenges and Opportunities Towards Decarbonisation. *E-Prime - Advances in Electrical Engineering, Electronics and Energy*, **1**; 100002

Sathyajothi, S., R. Jayavel, and A. C. Dhanemozhi (2017). The Fabrication of Natural Dye Sensitized Solar Cell (DSSC) Based on $TiO_2$ using Henna and Beetroot Dye Extracts. *Materials Today: Proceedings*, **4**(2); 668–676

 

Shenogin, S., L. Ferguson, and A. K. Roy (2020). The Effect of Contact Resistance on Electrical Conductivity in Filled Elastomer Materials. *Polymer*, **198**; 122502

Sinha, D., D. De, and A. Ayaz (2018). Performance and Stability Analysis of Curcumin Dye as a Photo Sensitizer used in Nanostructured ZnO Based DSSC. *Spectrochimica Acta - Part A: Molecular and Biomolecular Spectroscopy*, **193**; 467–474

Sundaramoorthy, K., S. P. Muthu, and R. Perumalsamy (2018). Enhanced Performance of 4,4-Bipyridine-Doped PVDF/KI/I2 Based Solid State Polymer Electrolyte for Dye-Sensitized Solar Cell Applications. *Journal of Materials Science: Materials in Electronics*, **29**(21); 18074–18081

Tayeb, A. M., A. A. A. Solyman, M. Hassan, and T. M. Abu el Ella (2022). Modeling and Simulation of Dye-Sensitized Solar Cell: Model Verification for Different Semiconductors and Dyes. *Alexandria Engineering Journal*, **61**(12); 9249–9260

Tomar, N., V. S. Dhaka, and P. K. Surolia (2021). A Brief Review on Carbon Nanomaterial Counter Electrodes for N719 Based Dye-Sensitized Solar Cells. *Materials Today: Proceedings*, **43**; 2975–2978

Twitchell, J., K. DeSomber, and D. Bhatnagar (2023). Defining Long Duration Energy Storage. *Journal of Energy Storage*, **60**; 105787

Venkateswari, R. and S. Sreejith (2019). Factors Influencing the Efficiency of Photovoltaic System. *Renewable and Sustainable Energy Reviews*, **101**; 376–394

Vidana Gamage, G. C., Y. Y. Lim, and W. S. Choo (2021). Anthocyanins from *Clitoria ternatea* Flower: Biosynthesis, Extraction, Stability, Antioxidant Activity, and Applications. *Frontiers in Plant Science*, **12**; 792303

Weldemicheal, H. T., M. A. Desta, and Y. S. Mekonnen (2023). Derivatized Photosensitizer for an Improved Performance of the Dye-Sensitized Solar Cell. *Results in Chemistry*, **5**(10); 100838

Xiao, K., L. Jiang, and M. Antonietti (2019). Ion Transport in Nanofluidic Devices for Energy Harvesting. *Joule*, **3**(10); 2364–2380

Yoo, S.-M., S. J. Yoon, J. A. Anta, H. J. Lee, P. P. Boix, and I. Mora-Seró (2019). An Equivalent Circuit for Perovskite Solar Cell Bridging Sensitized to Thin Film Architectures. *Joule*, **3**(10); 2535–2549

Zhang, H., W. Lu, and X. Li (2019). Progress and Perspectives of Fow Battery Technologies. *Electrochemical Energy Reviews*, **2**(3); 492–506

 